AD-A122 721 MECHANICS AND PRACTICE (SELECTED ARTICLES)(U) FOREIGN 1/1
TECHNOLOGY DIV WRIGHT-PATTERSON AFB OH P Y WANG ET AL.
17 NOV 82 FTD-ID(RS)T-1363-82

UNCLASSIFIED F/G 20/11 NL

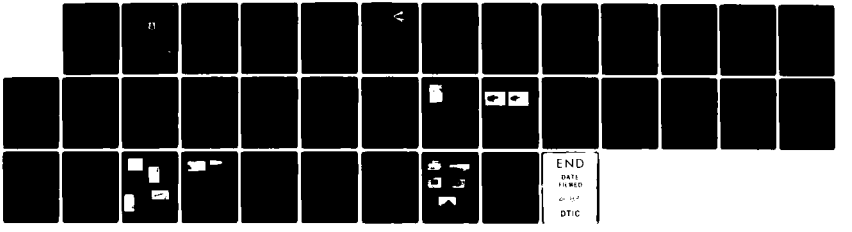

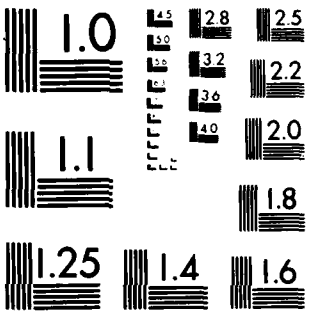

FTD-ID(RS)T-1363-82

AD A122721

FOREIGN TECHNOLOGY DIVISION

MECHANICS AND PRACTICE

(Selected Articles)

EDITED TRANSLATION

FTD-ID(RS)T-1363-82 17 November 1982

MICROFICHE NR: FTD-82-C-001479

MECHANICS AND PRACTICE (Selected Articles)

English pages: 32

Source: Lixue yu Shijian, Vol. 4, Nr. 2, 1982, pp. 17-21; 47-50; 55-58; 67; 71-72

Country of origin: China
Translated by: SCITRAN
F33657-81-D-0263
Requester: FTD/TQTA

PREPARED BY:

TRANSLATION DIVISION
FOREIGN TECHNOLOGY DIVISION
WP-AFB, OHIO.

Table of Contents

MECHANICS AND PRACTICE

THE ELECTROMAGNETIC EFFECT OF PLASMA SHEATH IN REENTRY FLIGHT

Wang Pao Yee
(Mechanics Institute, Academia Sinica)

I. INTRODUCTION

The so-called reentry plasma sheath is the high temperature ionized gas layer produced by shockwave compression and friction of the flight vehicle reentering the atmosphere (refer to Figure 1). It is closely related to the communication, guidance, remote measurement, detonation and electronic warfare problems of high speed vehicles. Therefore, it has attracted a lot of attention [1]; for example, the plasma sheath causes significant interference to the functions of the electromagnetic antenna system of the flight vehicle. It even causes the interruption of the communication which is commonly known as a blackout. In order to solve the blackout problem, one must rely on the knowledge in high temperature high velocity aerodynamics, electromagnetic fluid mechanics and plasma physics.

The studies on the reentry plasma sheath approximately began in the 60's. It involves a wide variaty of areas. From the point of view of the purpose of the study, it includes the ionization mechanism, electromagnetic effect and the alleviation measures [2], etc. From the depth of the studies, it ranges from the linear mutual interaction between low power electromagnetic waves with the plasma, up to the nonlinear reaction at high power [3,4]. From the broadness of the studies, it includes the decay of the signal, the penetration characteristics, up to the turbulent noise [5]. From the contents of the studies, the various antenna structures installed at different parts of the flight vehicle have been explored [6-8].

The relevant institutions abroad believe that the study of reentry communication is still one of the major topics in research on reentry systems in the next 10 years [9]. Since electromagnetic antennas are

also widely used as the diagnostic tool in studying the plasma of the universe, the Earth and in the laboratory [10]; therefore, this type of study has a more widespread meaning.

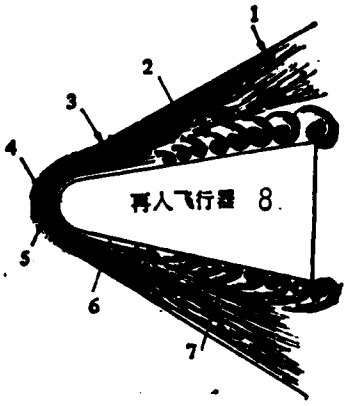

Figure 1. Schematic diagram of the structure of the reentry plasma sheath.
1--slanted shock wave; 2--nonviscous shock wave layer; 3--shock wave front; 4--ionization front zone; 5--stationary point zone with dense plasma; 6--cold inner boundary layer; 7--turbulent boundary layer; 8--reentry flight vehicle

II. THE ELECTROMAGNETIC EFFECT OF THE REENTRY PLASMA SHEATH

The reason for causing the blackout is because a great portion of the electromagnetic energy radiated by the antenna on the flight vehicle is absorbed or reflected by the plasma in penetrating through the plasma sheath. Furthermore, the presence of the plasma also changes the terminal characteristics of the antennas. It would cause the mismatch of the antenna resistance and distortion of the radiation pattern. When it is even more serious, the antenna may have a voltage break through. These are factors which greatly reduce the electromagnetic wave.

To discuss the possible effect created by the plasma sheath on the antenna characteristics, it is essentially a study on the propagation of electromagnetic perturbations in the nonuniform and unsteady plasma medium with boundary motion. In other words, it is the problem of mutual interaction between the electromagnetic wave and the plasma. The electromagnetic phenomena in the plasma are abundant [11]. Here,we only discuss several electromagnetic effects related to the antenna problems.

1. Sheath envelope effect

When the antenna comes in contact with the plasma sheath, its surface forms a space charge layer which is commonly called an ionic sheath envelope in which the density of the positive ions is greater than that of electrons. The distribution is nonuniform by height. It maintains

a negative potential (floating potential) and its thickness is on the same order of magnitude as the Debye shield length. This situation will not occur for antennas in free space. It is a plasma phenomenon which has been discovered in gas discharge and plasma diagnostic studies [12]. It has been analyzed in detail earlier [13,14]. If a direct current polarization potential is applied at a constant value to the antenna, then the plasma sheath envelope no longer exists. At this time, a uniform plasma is present near the antenna. This situation can be called the collapse of the sheath envelope [15].

The ionic sheath envelope not only increases the effective dimensions of the antennas, but also affects the radiation characteristics of the antennas [16]. For example, it changes the electrical conductivity and inductance of the aperture antenna (refer to Figure 2) [17]. Therefore, the sheath envelope effect should be taken into account when studying the antennas covered by plasma. For electronic plasma*, an abrupt free space thin layer can be used to approximate the ionic sheath envelope. In recent years, some researchers have been further considering the effect of inhomogeneous sheath envelopes [18].

2. Dispersion effect

One of the characteristics of the plasma is the significantly large frequency dispersion, which means that its dielectric constant varies with the frequency of the electromagnetic wave. For example, the equivalent complex dielectric constant of the electronic plasma is [19]

$$\varepsilon_p = \left[\left(1 - \frac{\omega_p^2}{\omega^2 + \nu^2}\right) - i\left(\frac{\omega_p^2}{\omega^2 + \nu^2}\right)\left(\frac{\nu}{\omega}\right)\right]\varepsilon_0$$

where $\omega_p = [n_e e^2/m_e \varepsilon_0]^{1/2}$ is the plasma frequency, ε_0 is the dielectric constant of the free space; m_e and e are the mass and the charge of the electron. Thus, the corresponding plasma propagation coefficient is

*Assuming the temperature of charged particles is not zero, it takes the effect of pressure expansion and thermal expansion due to thermal motion into account.

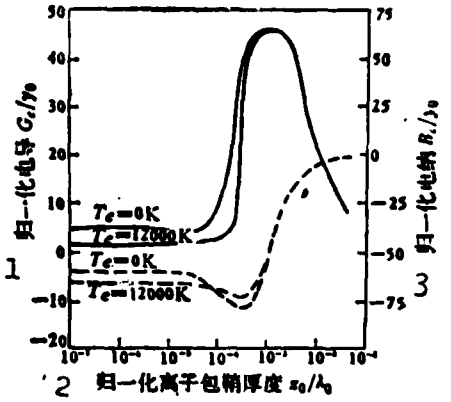

图 2 离子包鞘对矩形孔径天线导纳的影响
——电导，4 ——电纳 5
$(\omega/\omega_p)^2=0.1$, $\nu/\omega_p=0.01$,
$a/\lambda_0=0.01$, $b/\lambda_0=2$

Figure 2. The effect of ionic sheath envelope on the conductivity and inductance of a rectangularly shaped aperture antenna
1--normalized electrical conductivity z_e/λ_0; 3--normalized electrical induction B_e/y_0; 4--electrical conductivity; 5--electrical inductance.

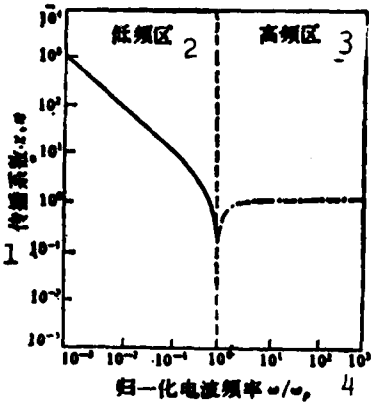

图 3 无碰撞等离子体的衰减率、折射率
——衰减率 χ, 5 ---折射率 6

Figure 3. The decay rate and refraction rate of collisionless plasma.
1--propagation coefficient; 2--low frequency region; 3--high frequency region; 4--normalized electromagnetic wave frequency; 5--decay rate χ; 6--refraction index n

$$\alpha_p=\frac{\omega}{c}\left[\frac{(K_r^2+K_i^2)^{1/2}-K_r}{2}\right]^{1/2}$$

$$\beta_p=\frac{\omega}{c}\left[\frac{(K_r^2+K_i^2)^{1/2}-K_r}{2}\right]^{1/2}$$

where $K_r=1-\frac{\omega_p^2}{\omega^2+\nu^2}$, $K_i=\frac{\omega_p^2}{\omega^2+\nu^2}\frac{\nu}{\omega}$. . From this, we can see that the propagation characteristics of the plasma is a function of the electromagnetic wave frequency. Here, ω_p is an important characteristic parameter. Usually the conditions of $\omega_p<\omega$ and $\omega_p>\omega$ are called less dense and overly dense plasma, respectively. $\omega_p=\omega$ is the critical plasma. The propagation characteristics in these three regions is quite different. For example, under collisionless conditions ($\nu = 0$) if $\omega = \omega_p$ then the electromagnetic wave does not propagate. It is totally reflected at the surface. Usually, this ω value is called the cutoff frequency. If $\omega > \omega_p$, then it is the high frequency region in which the electromagnetic wave propagates without decay but with phase shift. If $\omega < \omega_p$, then the electromagnetic wave decays exponentially. This is the low frequency region. Figure 3 provides the decay rate and refraction rate of the collisionless plasma as a function of frequency.

3. Effect of collision

When the charged particles in the plasma collide, part of the energy is transferred to the collided particle. Therefore, a collision may become an energy loss mechanism. Usually, this type of plasma is plasma with losses. In addition, collisions may cause the electrical conductivity of the plasma to be non-zero. Therefore, its propagation characteristics are also changed. When the electron collision frequency in the plasma is more apparent, its propagation characteristics are not quite the same as those in the collisionless situation (refer to Figure 4). At this time, in all the frequency regions, the electromagnetic wave propagates with decay. However, in the low frequency region, when the electromagnetic wave frequency is lower than the collision frequency, a decrease in wave frequency can decrease the decay [20].

4. The effect of compressibility

The compressibility of the reentry plasma sheath can produce significant affects on the antenna characteristics. This problem was discovered in the study of hot plasma* radiation source characteristics [21]. The electromagnetic antenna can be excited in a hot plasma and propagate a plasma wave form electro acoustic wave. This phenomenon was verified in the exploration of the ionosphere [22]. Therefore, it is widely looked upon in the study of reentry antennas [23]. People have even used it as the basis for the electroacoustic probes [24]. Furthermore, it was used to diagonize the reentry plasma sheath in experimental flights [25].

Because the temperature of the plasma is rather high, its pressure gradient effect cannot be neglected. When charged particles undergo forced oscillation under electromagnetic interactions, the pressure changes which causes the density of the charged particles to change. The propagation related to the alternating electric field of accumulation

*Assuming that the ions and neutral molecules are static, the electromagnetic characteristics of the plasma are determined by the electrons in motion in the background of the ions and the molecules. The effect of collision on the aperture antenna characteristics can be seen on Figure 5 in which the normalized collision frequency ν/ω_p is used as a parameter. It has a significant effect on the characteristic value of the antenna.

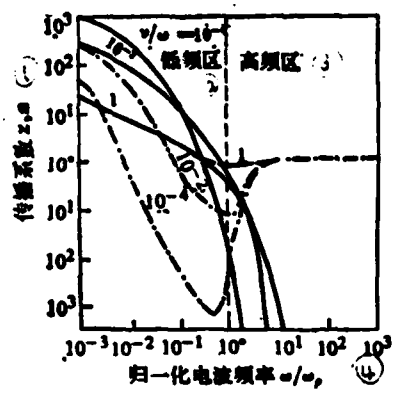

图 4 电子碰撞频率对传播特性的影响
——衰减率 χ, ⑤ ---折射率 n, ⑥

Figure 4. The effect of electron collision frequency on the propagation characteristics.
1--propagation coefficient χ,n; 2--low frequency region; 3--high frequency region; 4--normalized electromagnetic wave frequency ω/ω_p; 5--decay rate χ; 6--refraction index n

of charges is the electroacoustic wave. It is a longitudinal wave which propagates in the medium at the speed of sound. Due to the fact that some of the electromagnetic energy is transformed into the power of electroacoustic longitudinal waves (its ratio is determined by the antenna and the plasma condition [26], the antenna characteristics (represents the compressibility effect) on the characteristics of the aperture antenna is shown in Figure 5.

5. The effect of inhomogeneity

The reentry plasma sheath parameter has a certain spatial distribution. Its variational dimension is comparable to that of the wavelength of the electromagnetic wave. Therefore, the effect of an inhomogeneity must be considered. For most of the flight vehicles, the variation of the flow field parameter perpendicular to the surface is much steeper than that along the surface [27] (refer to Figure 6). Therefore, the plasma sheath can be treated as a plasma layered medium. Usually, it is approximated as a step-wise parallel homogeneous layered medium [28]. In addition, the structure and the installation of the antenna window will also cause some inhomogeneous factors [29,30].

The inhomogeneity effect is primarily shown in the reflection and refraction. These areas have been profoundly studied in the general theories of antennas [31,32].

6. The effect of boundary

The reentry plasma sheath is a finite region. Its inner edge is the surface of the flight vehicle. Its outer fringe is the wave front of the shockwave. Its thickness is on the order of 10-100 cm at most. In low altitude stationary point regions, it is even less than 1 mm.

Therefore, usually the boundary effect must be taken into account.

To discuss the boundary effect, it is not only necessary to provide the boundary conditions needed to solve the problem but also there are many interesting physical phenomena occurring at the boundary. In addition to the familiar phenomena such as refraction, reflection, scattering and diffraction as well as conditions such as surface wave excitation, stationary wave and resonance [33], it is also possible to have transformation and coupling [34] between different types of waves at the plasma boundary such as the transformation between the transverse electromagnetic wave and the electroacoustic wave.

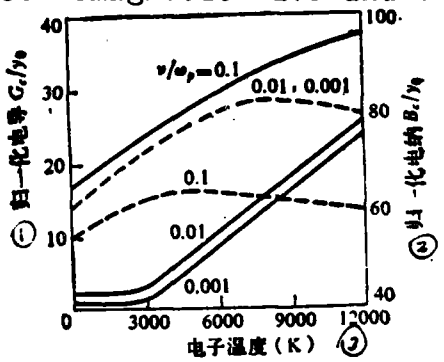

图 5 电子温度对矩形孔径天线导纳的影响
——电导④ -电纳⑤
$(\omega/\omega_p)^2=0.1$, $a/\lambda_0=0.01$, $b/\lambda_0=2$, $s_0/\lambda_0=3$

Figure 5. The effect of electron temperature on the rectangularly shaped aperture antenna
1--normalized electric conductivity G_0/y_0; 2--normalized electric inductance; 3--electron temperature; 4--electric conductivity; 5--electrical inductance

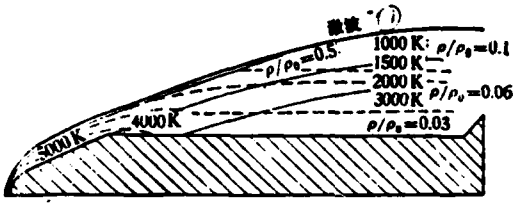

Figure 6. Typical parametric distribution of the reentry plasma sheath. (height 27 kilometer) [27]
1--shock wave

7. The effect of motion

The plasma sheath is moving at high speed relative to the flight vehicle and antenna. This type of motion can combine with the plasma wave to cause the transmission field and reflection field of the electromagnetic wave to change. When the direction of motion of the dielectric

and the polarization* of the incident wave are different, the effect of motion also varies. Furthermore, the plasma is acting as a dispersive dielectric. The effect created by its motion is greatly different from the results of an ordinary dielectric [35]. Figure 7 gives the relation between the reflection index R and the velocity of motion ($B = v/c$). It was the result of motion parallel to the boundary in an infinitely large homogeneous plasma, and the incident plane wave is parallelly polarized. Due to the changes of the reflection and transmission indices, the radiation pattern of the antenna is distorted; especially when $\omega \sim \omega_p$, the distortion is more obvious [36]. If the effect of compressibility and the magnetic field is simultaneously taken into account, the situation is even more complex [37,38]. Figure 8 shows the variation of the radiation pattern when $(\omega_p/\omega)^2 = 1.5$

8. The effect of ionization

The plasma can easily obtain large amounts of energy from the external field. Therefore, electromagnetic waves can heat up the plasma. The reentry plasma sheath is partially ionized by high temperature air. When the power of the electromagnetic wave of the antenna is large, it will cause excessive heating which leads to field induced ionization. This is the so-called antenna voltage break-through. The break-through will increase the degree of ionization of the plasma sheath. It will even change into an overly dense plasma which causes most of the power of the antenna radiation to be absorbed and reflected. The experiment indicates this nonlinear effect begins to appear even when the incident power is several hundred watts. Therefore, the high power electromagnetic wave transmission problem has attracted a lot of attention in recent years [39,40].

9. The effect of noise

*In the direction of the electric field vector of the maximum radiation of the antenna including circular polarization or linear polarization (perpendicular or horizontal).

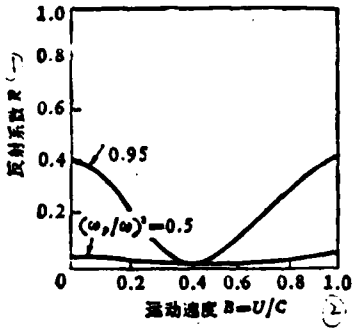

Figure 7. The effect of plasma on the propagation characteristics [35]
1--reflection index R;
2--velocity of motion B=U/C

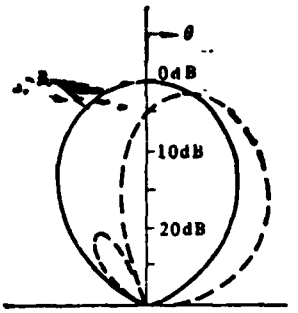

Figure 8. The effect of plasma motion on the radiation pattern of the antenna

—B = 0.0 —B = 0.4

The temperature of the reentry plasma sheath is very high. At the stationary point near the tip of the flight vehicle it can reach 10,000 K. At this time, the plasma itself can produce thermal radiation which forms noise. Flight experiments showed [41] that the noise voltage of the plasma can even exceed the stationary point temperature of the flow (refer to Figure 9).

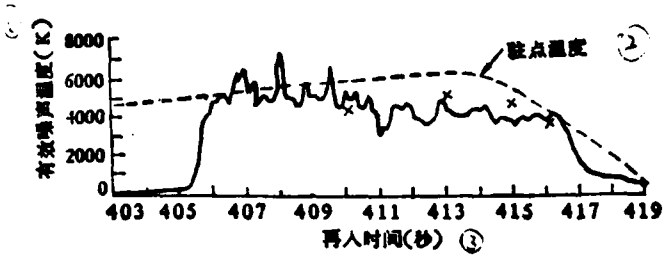

Figure 9. The effective plasma noise temperature at the antenna of a dull tip object [41]
1--effective noise temperature (K); 2--stationary point temperature;
3--reentry time (second)

In addition, the reentry plasma sheath is frequently a turbulent flow (especially in the rear flow field). This type of turbulent flow not only has microwave thermal radiation, but also can scatter part of the antenna radiated energy back [42]. These sources create noise. Of course, the turbulent plasma is an orderless medium in which the propagation of electromagnetic waves involves more problem. These problems will not be discussed here.

Table 1. χ band power of the reverse direction scattering by the turbulent flow

a(cm)	P_{rec}/P_{inc}
0.25	2.53×10^{-5}
0.79	0.93×10^{-6}
5	2.82×10^{-7}

where a is a relevant length of the turbulent flow. P_{rec} is the noise power and P_{inc} is the incident power.

III. CONCLUSION

The electromagnetic effects of the reentry plasma sheath are multiple. This paper only introduced part of them. Not only that the turbulent flow effect and the nonlinear effect are not described in detail, but also problems such as collisionless resistance, anisotropy effect and the propagation of electromagnetic pulses have not been dealt with. On the other hand, in an actual problem, it is not necessary to include all the effects described above. It may be simplified according to the actual conditions. For example, the effect of motion begins to have an apparent effect approximately at B = 0.1. In a reentry problem, the flight vehicle velocity is on the order of magnitude of 10 kilometers per second; therefore, the overall plasma sheath motion effect can be neglected. As another example, the turbulent flow scattered noise voltage under normal conditions is on the order of 50 dB,which is fairly small. Therefore, as long as it is taken into consideration in the multichannel communications system, it can be neglected. Even when analyzing the reentry antenna, it is frequently assumed that the plasma sheath is semi-infinite. For the propagation of electromagnetic waves in an overly dense medium, it is sufficiently accurate.

In summary, the study of reentry communication itself is an engineering realization problem. However, it involves antenna and electromagnetic wave propagation theories and many disciplines such as electromagnetic fluid mechanics and plasma physics. This reflects the mutual involvement of modern scientific technologies. It also demonstrated the application of fluid mechanics in engineering practice.

REFERENCES

[1] Wu chen kong. Plasma problems in High Speed Flights, Mechanics and Practice, 1 (1981), 2-7.

[2] Lennon, J. F. and Poirier, J. L., AD/A004046.

[3] Papa, R. J. and Taylor, R. L. Can. J. Phys. 53 (1975), 514-532.

[4] Rudderow, W. H., AD/A008514.

[5] Fante, B. L. AD756829.

[6] Cochrum, B. L. et al, AD/A024558.

[7] Bisplinghoff, R. L. et al, AD/A022683.

[8] Taylor, W. C., AD769957.

[9] Legendre, R. L. et al, Proceedings of the 24th International Instrumentation Symposium, May 1-5, 1978, Aubuquerque, New Mexico.

[10] Singh, R. N. AD774639.

[11] V.L. Kingsberg. Propagation of Electromagnetic Wave in Plasma (translated by Chien Shenjay), Science Publication, (1978).

[12] Langmuir, D. I. and Mott-Smith, H. Gen. Electr. Rev., 27 (1924), 449-455.

[13] Laframboise, J. AD634596.

[14] P. N. Hu and Ziering, S. Phys. Fluids, 9 (1966), 2168-2179.

[15] Wait, J. R. Can. J. Phys., 44 (1966), 293-302.

[16] Meyer, P. et al. J. Appl. Phys., 45 (1974), 700-706.

[17] Rybak, J. P. AD718981.

[18] Meyer-Vernet, N. et al. Radio Sci., 13 (1978), 69-73.

[19] Heald, M. A. and Wharton, C. B. Plasma Diagnostics with Microwave, John Wiley and Sons Inc., New York (1965).

[20] Rybak, J. P. and Churchill, R. J. IEEE Trans., AES-7 (1971), 879-894.

[21] Cohen, M. H. Phys. Rev., 123 (1961), 711; Phys. Rev., 126 (1962), 389.

[22] Whale, H. A. J. Geo. Res., 68 (1963), 415-420.

[23] Rybak, J. P. AD720262.

[24] istensen, T. et al. Radio Sci., 12 (1977), 935-939.

[25] Baird III, A. W. and Lusting, C. D. NASA SP-252 (1971), 57-64.

[26] Galejs, J. Radio Sci., 1 (1966), 457-474.

[27] Jackman, D. A. et al. Space/Aero., 41 (1964), 53-57.

[28] Hamn, J. M. and Tyras, G. Radio Sci., 1 (1966), 1263-1271.

[29] Siraprasad, K. and Celikkol, B. Can. J. Phys., 49 (1971), 2938-2946.

[30] Jones, J. E., IEEE Trans., AP-17 (1969), 63-68.

[31] Galejs, J. Antennas in Inhomogeneous Media, Pergamon Press (1969).

[32] Wait, J. R., Electromagnetic Waves in Stratified Media. Pergamon Press (1970).

[33] Rybak, J. P. et al. AD778828.

[34] Felsen, L. B. and Labianca, F. M. Radio Sci., 2 (1967) 29-71.

[35] Yeh, C. J. Appl. Phys. 37 (1966), 3079-3082; 38 (1967), 2871-2873.

[36] Casey, K. F. IEEE Trans., AP-19 (1971), 401-405.

[37] Kojima, T. et al. IEEE Trans. AP-20 (1972), 398-400.

[38] Kojima, T. and Higash, T. Radio Sci., 8 (1973), 1149-1155.

[39] Papa, R. J. and Taylor, R. L. AD766206.

[40] Rudderow, W. H. AD/A016449.

[41] Caldecott, R. et al. IEEE Trans., AP-17 (1969), 786-790.

[42] Fante, R. L. AD756829.

(translated by Chien Shenjay), Science Publication (1978)

MASS FLOW RATE MEASUREMENT IN ELECTRIC ARC WIND TUNNEL EXPERIMENTAL SECTION

Chin Chenyin, Chi Loanshi and Chu Kerli

I. INTRODUCTION

The total pressure, static pressure and mass flow rate of the air flow in the electric arc wind tunnel experiment section are the important parameters in the calibration of the experimental section flow.

Due to the inhomogeneity air heated in an electric arc, the nonuniform expansion in nonlinear nozzles, the cooling affect of the nozzle wall and the affect of the absorbing layer of the nozzle wall, the flow parameters are nonuniformly distributed along the radial direction of the flow in an experimental section. In the meantime, due to the divergence effect of the conically shaped nozzle, the flow parameters also vary along the axial direction of the flow. Hence, the nozzle exit parameters calculated according to the one-dimensional isoentropic equations are different from the actual parameters. In order to accurately calibrate the flow parameters in the experimental section, it is necessary to use a probe to measure point by point. This paper discusses the measurement of mass flow rate of a wind tunnel experimental section. The probe for this type of measurement is called a ρu probe.

According to the mass flow rate ρu, of the experimental section, the flow static pressure p_1 in front of the shock wave and the total pressure p_{T_2} behind the shock wave, it is possible to calculate the flow velocity u_1 and density ρ_1.

There was a report on the measurement with the ρu probe abroad as early as the 50's [1]. Krause mentioned in an article regarding ρu probe measurements that up until the 70's, this type of work was still carried out abroad. The major studies were on the applicable range of the probe and the miniaturization of the probe [2].

We developed a set of ρu probes with gas inlet diameter of 1 mm and carried out experiments in a 1.5 megawatt electric arc heated air supersonic wind tunnel. The reliability of this type of probe as a supersonic measurement tool has been verified. Using these probes, the mass flow rate ρu on the three cross-sections along the experimental section and the total pressure p_{T_2} were obtained. Using these data, the velocity and density of the flow were calculated.

II. PRINCIPLE OF THE MEASUREMENTS

The mass flow rate probe is a tube with a sharp front beak placed in the supersonic flow. Let us assume that in the experimental section the probe is placed in a small flow under the local supersonic conditions. According to the continuity equation, we get

$$\dot{M} = \rho u A \qquad (1)$$

where $\dot{M}$ is the mass of gas sucked into the probe in unit time, ρ is the local flow density, u is the local flow velocity, and A is the cross-sectional area of the front beak of the probe. Therefore,

$$\rho u = \dot{M}/A \qquad (2)$$

The amount of flow $\dot{M}$ passing through the probe in unit time can be pre-calibrated by measuring with a Lafarer nozzle. The cross-sectional area of the front beak of the probe can also be determined ahead of time. Using equation (2), the value of the mass flow rate ρu can be calculated.

The ρu probe operates in a supersonic flow environment. In order to accurately determine the unperturbed incoming flow, it is necessary to satisfy the two following conditions: i.e., 1) the flow must enter the probe as a free flow at supersonic speed; 2) the flow cross-section sucked in by the probe must be the same as the geometric cross-section of the front beak inlet of the probe. In order to form a supersonic flow at the probe inlet, it is necessary to guide away the subsonic flow behind the normal shock wave formed in front of the probe. To accomplish this objective, it is necessary to carry out the verification of plugging near the probe inlet section and the calculation of the resistance loss of the flow along the tube of the probe. In order to satisfy the latter condition, we must shape the front beak in the shape as shown in Figure 1 which is an equi-angle sharply cleaved shape.

The supersonic flow produces two slanted shockwaves at an equal angle on both sides of the sharp cleavage. The incoming flow streamline is symmetrically divided at the tip. The result is that the flow beam entering the probe is not disturbed which is identical to a free flow beam with a cross-sectional area A [3].

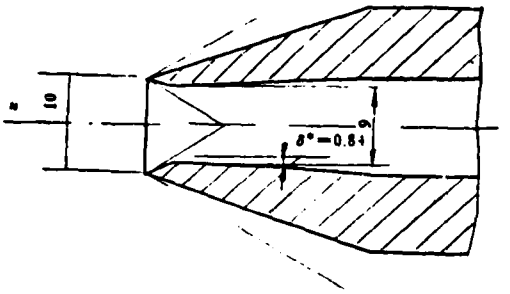

Figure 1. Flow pattern near the inlet of the ρu probe

III. THE FLUID MECHANICAL DESIGN OF THE ρu PROBE

The fluid mechanical design of the ρu probe includes the following parts:

1. Estimation of the parameters to be measured. Use a set of theoretical estimation values of a typical wind tunnel experimental section flow parameters as the original basis of probe design. We choose the diameter of the outlet of the wind tunnel nozzle to be 20 cm, the total enthalpy h_s of the flow to be 12.6 mega joule/kg, the flow state pressure ρ_1 to be 10 Newton/m^2, the flow density ρ_1 to be 0.186 x 10^{-3} kg/m^3, flow velocity u_1 to be 4550 m/sec and the gas mass flow rate $\rho_1 u_1$ to be 0.845 kg/m^2 sec.

2. Selection of the geometrical parameters of the probe. The inlet of the probe is of a compressible expansion type by taking the plugging problem into consideration and to assume that the probe has a certain distinguishability. Let us choose the front beak diameter to be 1 cm, the minimum cross-section diameter to be 0.9 cm, the distance between the tip of the probe to the throat to be 0.4 cm, the front beak half angle to be 20°, gas tube length to be 50 cm and the inner diameter of the tube to be 1 cm.

3. Calculation of the probe inlet parameters. Use the parameters behind the normal shockwave under typical flow parameters as the probe inlet parameters. Apparently, this set of inlet parameters is the least favorable condition to establish a supersonic flow in the probe tube.

4. Verification of plugging of the inlet section. Estimate the effective contraction ratio of the inlet section and compare it with the theoretical contraction ratio.

5. Calculation of the tube flow. Use Reynolds' simulation method and the resistance coefficient method to calculate the parametric variation of the flow along the tube by sections to obtain the probe outlet parameters [5].

6. Estimation of the measurement nozzle throat. Use the equation introduced in [4]

$$\dot{M} = 410 A_n^* \frac{P_0}{\sqrt{T_0}} \qquad (3)$$

to estimate the throat of the measurement nozzle A_n^*.

7. Estimation of the air suction pump system. Choose the 2x-6 vacuum pump as the air suction apparatus of the ρu probe system and perform volumetric calibration.

IV. STRUCTURAL DESIGN OF THE ρu PROBE

The probe itself adopts a water cooled triple tube structure. In order to increase the cooling effect of the inner wall of the probe front beak, the front beak inner wall is equipped with a water supply to make the local water flow rate not less than 1 m/sec. The curved part of the probe tube uses a 4.0 cm radius elbow to make a smooth transition in order to reduce the local resistance loss of the flow. Figure 2 gives the external look of the fabricated ρu probe.

V. STANDARDIZATION OF THE MEASUREMENT NOZZLE

The Lafarer nozzle used to measure the value of ρu should be standardized before the experiment. We used a constant volume standardization method to obtain the curves showing the relations between the amount of flow and the upstream pressure of the nozzle throat and temperature. It was proven by practice that ensuring a smooth nozzle streamline and maintaining a sufficient polishing condition of the inner wall of the

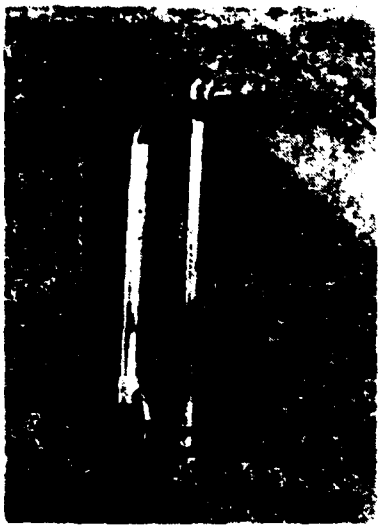

Figure 2. External look of the ρu probe

nozzle would be the key to maintaining stability in the effect cross-sectional coefficient of the nozzle.

VI. TESTING OF THE PROBE

The ρu probe is tested in a 1.5 mega watt electric arc wind tunnel. Using a photographic method and a pressure drop method, whether the flow is entering the probe at a supersonic speed was determined.

1. Photographic method. Under two completely different experimental conditions, the flow patterns near the tip of the probe were photographed. One was to completely shut off the valve in the rear of the probe, and the other one is to open it all the way as shown in Figures 3(a) and 3(b). Photograph 3(a) shows the condition under which the rear valve was completely closed. We observed that there was a bright and unclear area forming. The bright area was the high temperature subsonic region behind the off-body shockwave. Photograph 3(b) shows the condition under which the rear valve is completely open. We can see the clear boundary in front of the probe. There was no bright area, indicating that supersonic flow was sucked into the inlet.

2. Pressure drop method. Using the variation of the pressure distribution inside the probe, whether the flow enters the probe at a supersonic speed can be determined. As shown in Figure 4, the pressure drop S between points A and B upstream from the throat of the measurement nozzle can be obtained in normal mass flow rate experiments. Choose another point C and change the gas flow tube cross-section at point C to change the pressure drop between points A and B. At this time, observe the variation of the back pressure ρu upstream of the throat of the nozzle. We could see that when S rose from 5 mm silicone oil volume height to 40 mm silicone oil volume height, ρu was virtually unchanged. This showed that the gas flow entered the probe at a supersonic speed. When the resistance of the tube changes, the pressure distribution inside the tube made corresponding

adjustments. However, the mass flow rate remained unchanged.

The results of both test methods were identical, i.e., gas flow was entering the probe at supersonic speeds.

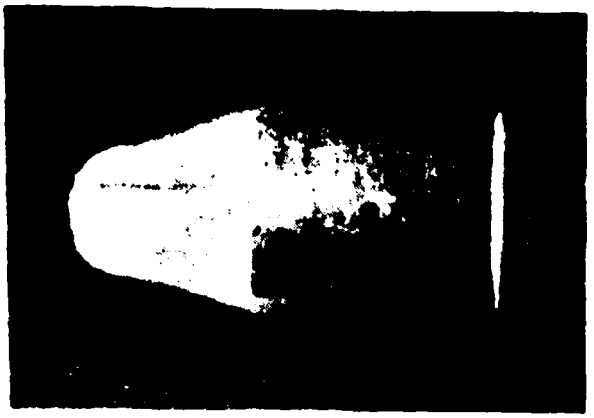

Figure 3(a). Photograph of the flow pattern at the tip of the ρu probe (rear valve closed)

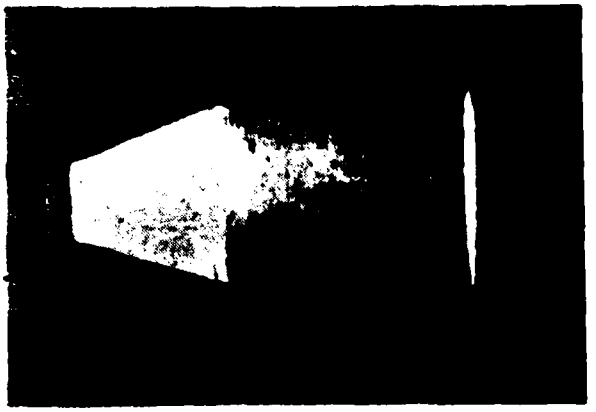

Figure 3(b). Photograph of the flow pattern at the tip of the ρu probe (rear valve open)

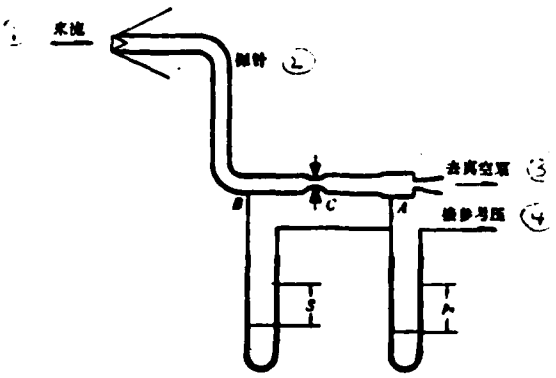

Figure 4. Experiment to determine supersonic flow speeds using a pressure drop method-
1--incoming flow; 2--probe; 3--to vacuum pump; 4--to reference pressure

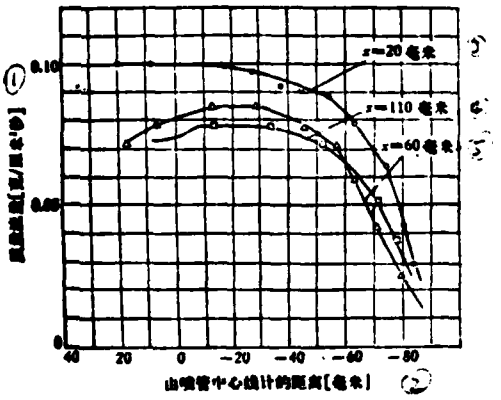

Figure 5. The mass flow rate ρu in the cross-sections of the flow in the wind tunnel experimental section.
1--mass flow rate (g/cm^2 sec); 2--distance from the center of the nozzle (mm); 3-- x=20 mm; 4--x=110 mm; 5--x=60 mm

VII. MEASUREMENT OF THE ρu PROBE

The ρu probe reported in this paper has been used to measure the gas flow in a 1.5 mega watt electric arc wind tunnel experimental section. In the experiment, the upstream pressure pn of the nozzle throat was measured using a capacitive voice type of pressure transducer. The temperature T_n in the upstream of the nozzle throat was measured using a copper-constantan thermocouple. The measured results are shown in Figure 5 which shows the mass flow rates along the three cross-sections of the flow. The maximum relative error of the measurement was ±6%.

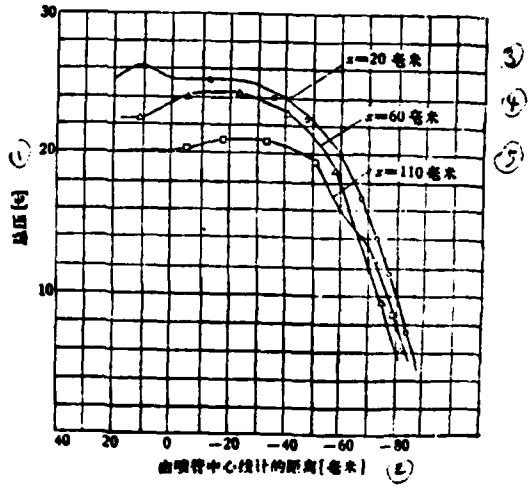

Figure 6. Total pressure at the cross-sections of the flow in the wind tunnel experimental section
1--total pressure (torr); 2--distance from the center of the nozzle (mm); 3--x=20 mm; 4-- x=60 mm ;5--x=110 mm

When the rear valve is closed, the ρu probe can also be used as a total pressure probe. Figure 6 shows the distribution of the total pressure P_{T_2} behind the shockwave in the three cross-sections along the gas flow obtained using this method. The measurement error was not greater than ±1%.

The measurements of ρu and P_{T_2} can be used to calculate the velocity and density of the gas flow. The appendix of [5] provided an approximation method as follows:

$$u_1 = \frac{(p_{T_1})_{\text{measured}}}{(\rho u)_{\text{measured}}}$$

$$\rho_1 = (\rho u)_{\text{measured}} / u_1$$

Based on the data already obtained, at a distance 20 mm away from the outlet of the wind tunnel nozzle, the velocity was 3800 m/sec and the density was 0.25×10^{-3} kg/m^3 ,using the above approximation equations.

VIII. CONCLUSION.REMARKS

This paper discussed the design and experimental problems for the ρu probes. After supersonic experimental verification, it was proven that the presently available 1 cm diameter ρu probe could operate normally in a supersonic flow whose total enthalpy was 12.6 mega joule/kg, total pressure in front of the wave was 1×10^6 Newton/m^2 and Mach number was 5. To determine the applicable range of the probe, more exploratory work is to be carried out.

The measurement results indicate that the major source of error in the measurement of ρu is the measurement nozzle. In order to raise the accuracy, first we must simplify the standardization of the nozzle.

In order to improve the distinguishability of the probe, it is necessary to study the miniaturization problem. Under low Reynolds' number conditions and when using a small probe, it is necessary to prevent the thickening of the absorbed layer to show a plugging phenomenon.

When the ρu probe measurement moves towards the high Mach number, the interaction between the shockwave and the surface absorbed layer can no longer be neglected.

Before the paper was published, we already saw the work done in the area of mass flow rate probe measurements by Comrade Chen Binyee. Comrade Chen Binyee directly used a volumetric method as the measurement technique of the probe and also used the rise of the pressure curve as the means to determine shockwave drawing. In addition, he analyzed the Reynolds' affect of the effective cross-section of the inlet.

All the work in this paper was performed under the guidance of Wu Chengkang. It also received some instruction from Ben Yingua.

SYMBOLS

A	cross-sectional A of the probe inlet
A_n^*	measurement nozzle throat
h	enthalpy
M	Mach number
$\dot{M}$	mass of gas passing through the probe per unit time
p	pressure
p_T	total pressure behind the wave
T	temperature
u	gas flow velocity
x	distance away from the outlet of the wind tunnel nozzle
δ	thickness of the absorbed surface layer
ρ	flow density
ρu	mass flow rate

Subscripts:

s	stagnation condition
1	static condition in front of the shockwave
2	condition behind the shockwave
n	condition in the upstream of the measurement nozzle throat

REFERENCES

[1] Jaskowsky, N. V., Some probe Measurements in the plasma Tunnel, PLR-8 Plasma-dyne, Corp., Jan. (1959).

[2] Krause, L. W. and Glawe, G. E., A Review of the mass-flux probe, NASA Lowis Research Center (1974).

[3] Huber, J. A. et al., Prbes for Measuring mass flow, Stagnation point heating and total enthalpy of high temperature gas flow, AIAA paper, No. 66-750 (1966).

(This paper was received on May 28, 1980)

THE FLUORESCENT MICROFIBER METHOD--A NEW METHOD TO OBSERVE THE FLOW PATTERN NEAR THE SURFACE OF AN OBJECT

Wong, Tzeshin and Wu Gunchin
(Nanjing Aeronautical Institute)

As for the methods used to observe the flow pattern on the surface of an object in a wind tunnel, a silk thread method or an oil flow method is commonly used. The silk thread method is only applicable to low velocity wind tunnels. Because the silk threads are relatively thick, there is more interference on the flow which affects the validity of the experimental results. Furthermore, it is impossible to densely adhere cloth on the object surface which makes it impossible, in many instances, to observe the complete flow pattern. The oil flow method, although it is applicable to high velocities and it is also possible to obtain the complete flow pattern, yet it pollutes the wind tunnel. Furthermore, if we wish to observe the flow pattern of the model under another condition, the cloth must be reprepared,which takes time. This is not economical for high velocity wind tunnels. The interpretation of the oil flow pattern also requires some experience; otherwise it is easy to misjudge the data.

We have successfully developed a new method to observe the flow pattern--the fluorescent microfiber method, which involves the use of fluorescent material synthetic fiber tape made by fibers 0.01-0.02 mm in diameter in the experiment. The dimension of this type of fiber is extremely small so that it can retain the accuracy of the model and has very little effect on the experimental results. These fluorescent fibers are barely visible under ordinary light to the naked eye. However, under ultraviolet light, they are very bright, which makes the diameter of the fiber appear to be several tens or over 100 times longer. This makes the observation and photographic recording of the record much easier.

I. INTRODUCTION OF THE METHOD

1. Fluorescent microfiber

Choice of material. The microfiber material must have sufficient strength. It is possible to use 0.01-0.02 mm diameter nylon fiber or equivalent. In order to facilitate the adhesion, the length of the fiber should be not less than 500 mm.

Fluorescence treatment. There are two methods of fluorescence treatment. One is to use a suitable fluorescent dye to color the fiber. However, because the surface of synthetic fiber is extremely smooth, it is very difficult to directly coat the fluorescent material onto it. Another method is to convert fluorescent material into fiber material and then draw the fine fiber.

Softening and antistatic treatments. Although the diameter of the nylon fiber is small, yet due to its high elastic modules it still is too stiff after it is cut short. It must undergo a softening process to improve the floating characteristics in the flow. In the meantime, the microfiber and the flow are in constant friction which would cause the accumulation of static electricity to lead to mutual attraction or adhesion to the model surface. Therefore, it is necessary to carry out an anti-static treatment.

2. Pasting method

For low velocity wooden models, the microfiber can be pasted using oil. The density of pasted fiber depends on the size of the model and the flow frequency type under observation. For larger models, the spacing can be larger and the microfiber can be longer. In the observation of the flow of off-body vortex of a triangular wing, the pasted fiber should be short and dense. In order not to let the microfibers tangle with one another, we believe that the length to spacing ratio should be 2:1 for good results. During pasting, it is necessary to choose straight and untwisted microfiber.

For high speed metallic metal, no. 20 glue can be used. The microfiber can be wiped off by a soft cloth and some solvent.

3. Light source

The microfibers we chose can fluoresce under the illumination of 3371Å-3650Å ultraviolet light. In the experiment, we used a reflection type dark high pressure mercury lamp whose main wavelength is 3650Å. The power required should depend on the area of the observation, size of the model and the spacing distance. The installation of the light source should minimize the reflection or direct incident of the ultraviolet light to the observer (a camera). Therefore, the light source should not be on the same side as the observer or the camera. It is most suitable to form a 30° angle between the emitted ultraviolet source from the light source and the line of visual (or the directive of the camera).

4. Photographic recording

Although the fluorescent microfiber can emit visible light under the illumination of ultraviolet light, yet the surroundings should still not be too bright to avoid affecting the observation and recording. Ordinary photography was used to do the photographic recording. No addition light source is needed,otherwise it is impossible to show the fluorescence vividly. In order to prevent ultraviolet light being reflected into the lens to smear the negative, the camera should have an ultraviolet filter added to it. Usually, 21° DIN film was used. After adding the ultraviolet filter, the f stop 4 and 1/10 sec speed could obtain satisfactory photographs.

5. Requirements for the surface of the model

The surface of the model should have minimal reflection. For metallic models, they should not be polished. For painted models, low reflectance paint should be used. The color of the paint should be different from the fluorescent color.

II. THE FLOW PATTERNS OF SEVERAL WING MODELS OBSERVED USING THE FLUORESCENT MICROFIBER METHOD

Experimental results (see Figures 1-6, in which the experimental conditions for Figures 1-5 were wind speed = 28 m/sec, Re = 3.8×10^5) indicate that the fluorescent microfiber technique can clearly distinguish the flow conditions flowing through the wings. If the fluorescent microfibers adhere to the surface along the flow, then it indicates that adherent flow exists in that location. At the tips of the wing, the microfibers show some deviation towards the outside in a regular pattern. In the outer side zone, it appears to be triangular,which shows that that area is affected by the wing tip vortex. Along with increasing tilt angle, it is possible to observe the expansion of the wing tip vortex affected zone. In the region where the microfibers swing slightly, it is the region that slight separation of gas flow occurs. In the photograph, the tails of the microfibers appear to be unclear. The microfibers appear to be erected or inverted in the severe separation region. In the photograph they appear to have a reverse hook. At the off-body vortex of the triangular wing and the side fringe vortex of the side fringe wing, the microfibers clearly show deviation in a regular manner. The direction of deviation is related to the direction of rotation of the vortex. The boundary with the surrounding unaffected area is very clear.

When the model posture changes, the pasted microfibers on the surface of the model also change the microfiber posture. When the model returns to the original posture, the microfiber posture is also restored. Based on this, the fluorescent microfiber method is direct and easy to read for the observation of the flow pattern on the surface. It is especially convenient to determine separation flow motion as well as easy for repeated experimental observations.

III. COMPARISON WITH THE WIND TUNNEL EXPERIMENT

In order to verify the effect of the pasted microfibers on the wind tunnel force measurement experiment data, we carried out comparison tests in high and low speed wind tunnels. The low speed test was carried out in the 1 m low speed wind tunnel at Nanjing Aeronautical Institute. The experimental model was a rectangular shaped wing with a chord length

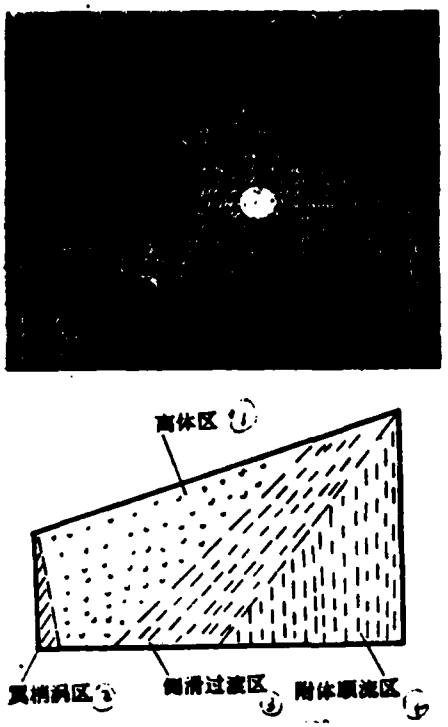

Figure 1. Trapezoidal wing $\alpha = 10°$
1--separation zone; 2--wing tip vortex zone; 3--side smooth transition region; 4--adherent smooth flow region

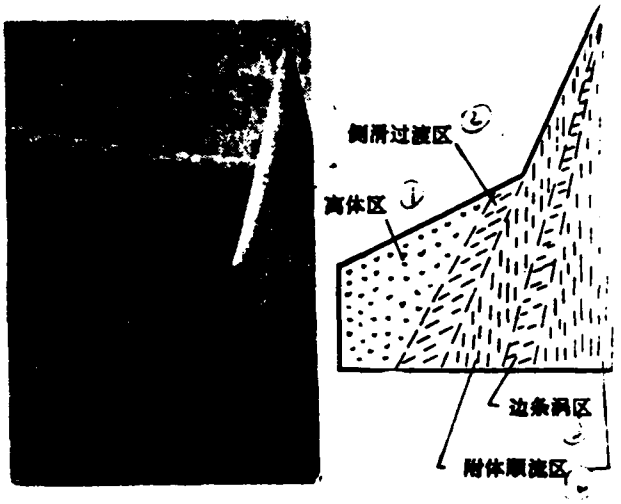

Figure 2. Side fringe wing $\alpha = 10°$
1--separation region; 2--side smooth transition region; 3--side fringe vortex region; 4--adherent flow region

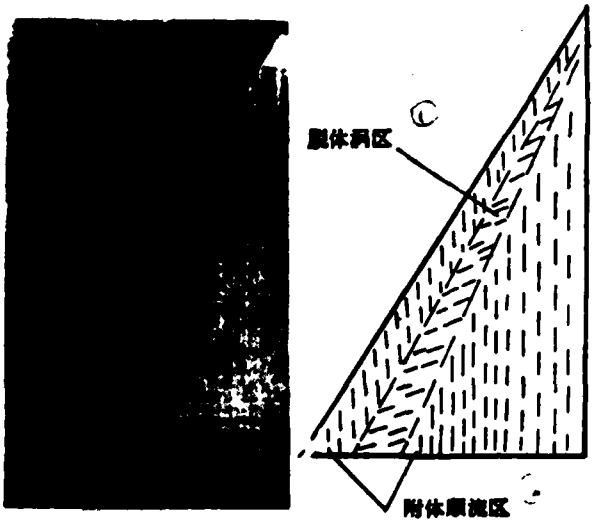

Figure 3. Triangular wing $\alpha = 10°$
1--separation vortex region; 2--adherent flow region

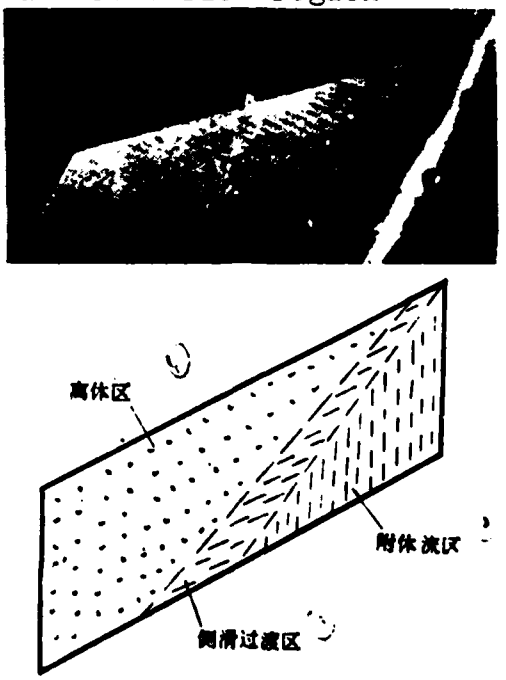

Figure 4. Rear glance wing $\alpha = 10°$
1--separation region; 2--adherent flow region; 3--side smooth transition region

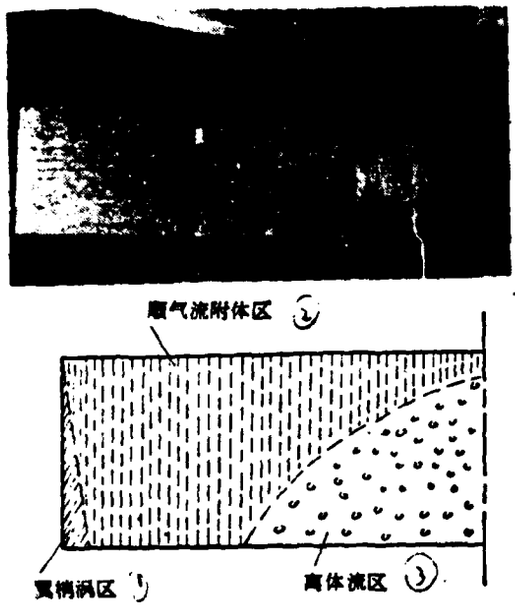

Figure 5. Rectangular wing
$\alpha = 14°$
1--wing tip vortex region;
2--adherent region along the flow; 3--separation flow region

Figure 6. Flow pattern of the plane tip at M = 0.85

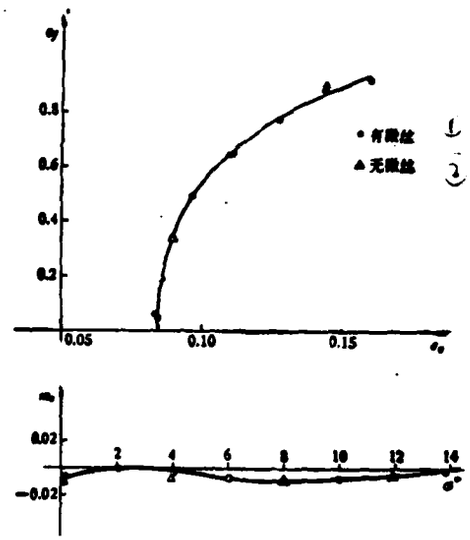

Figure 7. Comparison of experiments with and without microfibers in a low speed tunnel, C, light coefficient, C_x resistance coefficient, m_z longitudinal torque coefficient

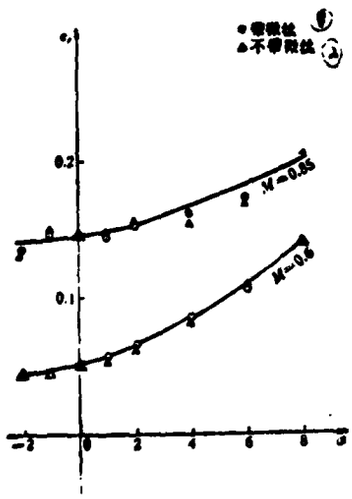

Figure 8. C_y-α curve when M = 0.6 and 0.85
1--with microfiber;
2--without microfiber

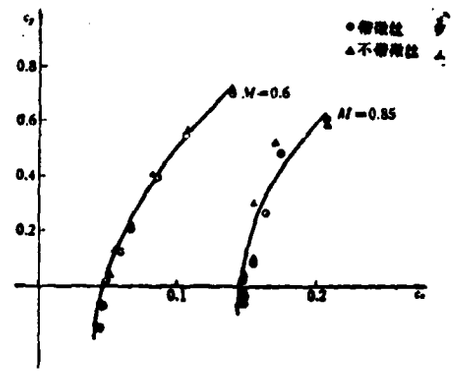

Figure 9. The C_y-C_x curve at M = 0.6, 0.85
1--with microfiber;
2--without microfiber

of 120 mm and a span of 700 mm. There were approximately 1000 microfibers pasted on the surface of the wing. The experimental results are shown in Figure 7. The high speed experiments were carried out in the high speed wind tunnel at Nanjing Aeronautical Institute. The experimental models were semi-models. Approximately 1000 microfibers each were pasted on the plane head, vertical tail wing and horizontal wing. The wing shape is rectangular. The span of the half wing is 300 mm and chord length is 150 mm. The experimental Mach number is 0.85. The experimental results are shown in Figures 8-9.

From the results above, it can be concluded that at low speed the experimental difference between with microfiber and without microfiber is very small and it is within the experimental error. At high speeds, the results before and after microfiber pasting are also pretty consistent. The effect on resistance is also very small, well within the experimental error. Therefore, the effect on the experimental result is negligible.

In the high speed experiments, because the microfibers are so thin that many of them were broken in the wing separation region. The other parts did not detach after four minutes of continuous high speed wind.

IV. CONCLUSIONS

The fluorescent microfiber method is an advanced method to observe in real time and to record flow patterns under various flow conditions. It does not affect the aerodynamic characteristics of the model and does not pollute the wind tunnel. It can be used to observe the flow pattern in large Re number and large M number conditions. Simultaneously, the force measurements can be carried out. The flow patterns obtained are direct and clear. It is convenient to observe the flow pattern variation with continuous changes of model posture, especially for high speed wind tunnels. It drastically saves the experimental time which is facilitating the improvement of designs.

REFERENCES

[1] AIAA paper 79-1877 Aircraft Systems and Technology Meeting, August 20-22, New York (1979).

(This paper was received on May 13, 1981)

TWO DIMENSIONAL WATER TUNNEL FLOW DISPLAY

Lo Minghwai and Who her

In recent years, the experimental techniques of using various types of water tunnels and water sinks to carry out flow displays abroad have received wide spread application and development. The photographs of the flow patterns obtained have clear patterns, are easy to distinguish and are colorful.

The Mechanical Institute of Academia Sinica built a flow pattern laboratory (Photograph 1) at the end of 1979 to be dedicated to flow display experiments using water medium equipment. The laboratory was equipped with a low speed two dimensional open water tunnel, a small water sink and a flow pipe. At the present moment, the two dimensional water tunnel has been operational and lots of experimental photographs were taken. The experimental flow diagram starts from the water reservoir to the adjusting valve, the flow meter, the diffusion section, to enter the flow stabilization section. In the flow stabilization section, through the use of a flow regulating net, the water flows through the contraction section to enter the experimental section. Finally, the water is ejected from the diffusion section.

Water reservoir: There are two sealed cylinders. The diameter is 1 m, 3.2 m long and 2.5 cubic meters in volume. They were welded by stainless steel sheets. They can contain 5 tons of water. The water tanks are installed with water supply pipes, over flow pipe, water discharge pipe and water transport pipe. Compressed air pipe was also installed to establish a 2 mPar pressure in the tank using compressed air.

Diffusion section: It is a round to square design. The inlet is a ϕ100 circle and the outlet is a 450x450 square. The diffusion angle is 45°. It is welded using stainless steel sheets. The two sides were connected using flanges.

Flow stabilization section: The inlet is a 450x450 square. It was glued together using 20 mm thick organic glass. Three no. 20 nylon nets

Photograph 1

Photograph 2

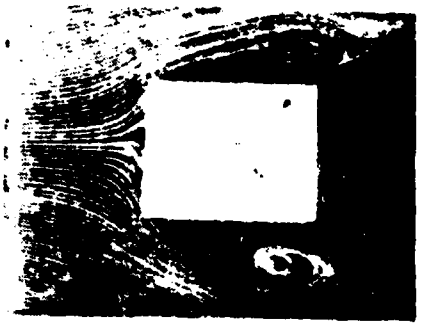

Photograph 3

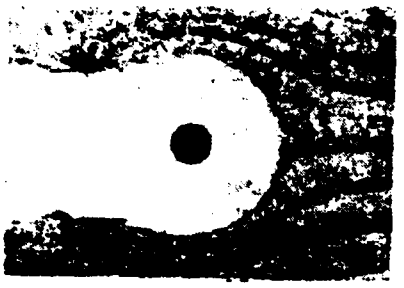

Photograph 4

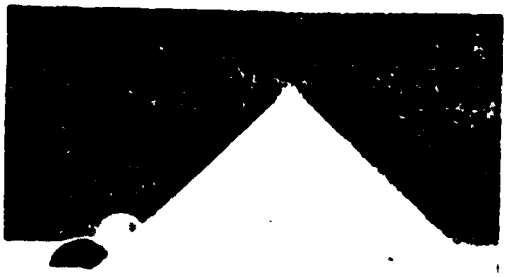

Photograph 5

and one no. 50 copper net are installed inside the flow stabilization section.

Contraction section: The inlet is a 450x450 square and the outlet is a 450x40 rectangle. It was glued together using 20 mm thick organic glass plate.

Experimental section: Its cross-section is a 450x40 rectangle with a total length of 3 meters. The four walls were glued together using 20 mm thick transparent organic glass plates. The two sides were polished inside and out to facilitate illumination for photography. On the other side, there is a rectangular window which is used to load and unload the models. The flow speed range in the experimental section is 3-50 cm/sec. The maximum Reynolds number is 7.28×10^4.

In this apparatus, we presently employed three display methods, i.e., color solution direct injection display method, wall surface coating display method and hydrogen bubble display method. The display solutions used are ink, food coloring and milk. Alcohol was used to adjust the specific gravity. The electrodes used in the hydrogen bubble method are 5-20 μ tungsten wire and platinum wire. The applied voltage is dc 100 to 400 volts,which is adjustable. The electrodes are linear and sawtooth shaped. Using these methods, the flow displays of the steady and nonsteady flow around cylinders, sharp angles, sharp tips and plates were obtained and black and white and color pictures of the flow patterns were taken.

The typical plate unsteady flow pattern is shown in Photograph 2. (Wall surface coating display method). Photograph 3 is the flow pattern of steady flow of the cubical model (hydrogen bubble method). Photograph 4 is the flow pattern of river flow of the boundary layer of a cylinder (color solution direct injection display method). Figure 5 is the flow pattern of the nonsteady flow for a sharply angled model (color solution direct injection display method).

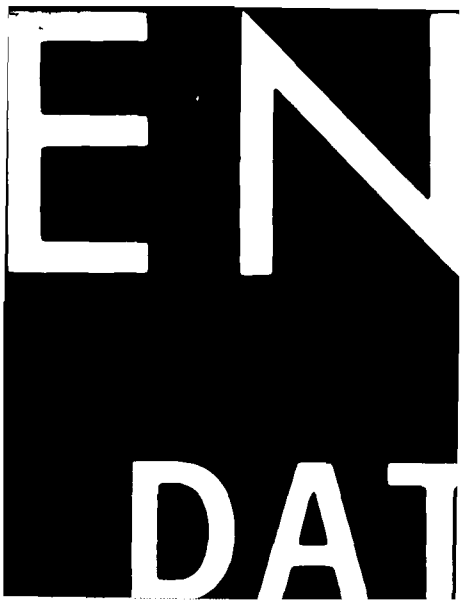
EN
DAT